Appl. Phys. B 62, 503–510 (1996)

Applied Physics B Lasers and Optics

Imaging and analysis of photomechanical effects induced in water by high-power laser–target interaction

S. Siano, R. Pini, R. Salimbeni, M. Vannini

Istituto di Elettronica Quantistica, CNR (Italian National Research Council), Via Panciatichi 56/30, I-50127 Florence, Italy
(Fax: + 39-55/414612, E-mail: RPINI@mailbox.ieq.fi.cnr.it)

Received: 2 March 1995/Accepted: 29 September 1995

Abstract. The kinetics of cavitation and associated photomechanical effects induced by underwater pulsed-laser irradiation of solid targets has been studied experimentally and analyzed with theoretical methods. A xenon–chloride excimer laser of 150 ns pulse duration has been utilized to produce ablation and local photofragmentation of artificial samples of hard tissues at fluences of 12–24 J/cm^2. The evolution of pressure wave and cavitation formations developing in the liquid from the target surface after laser irradiation has been observed with a time-resolved imaging technique employing a pump–probe laser arrangement. The analysis of experimental results has been performed by using the theoretical model of "point explosion" that has been successfully applied to fit the cavitation kinetics, providing also quantitative information on the energy transfer during photoacoustic interactions.

PACS: 42.80; 81.60; 42.55

Medical applications of photoacoustic and photomechanical effects induced underwater by pulsed radiation of high-power lasers on organic tissues have been proposed in the last decade and used clinically in surgical procedures as laser lithotripsy [1–3] and ophthalmology [4–6]. On the other hand, the explosive nature of laser–tissue interaction has been recently recognized also in medical treatments utilizing laser ablation of tissue at lower fluence levels [7–9]. In these cases high-pressure waves and cavitation formations originated by laser irradiation can represent a complexity of the laser treatment, producing mechanical stress or laceration into tissue.

Laser-induced photoacoustic effects, enhanced by the confinement in the liquid medium [10], are being investigated also in some material processing techniques, as laser cleaning of industrial products [11] and restoration of artistic sculptures and stained glass windows [12].

Well before raising interest in the application of such processes in biomedical and material processing fields, basic researches had put in evidence for the main physical processes involved in underwater high-power laser–target interaction [13, 14]. The different phases typically occurring in sequence, can be summarized as plasma initiation and its supersonic expansion, pressure wave formation, and cavitation mechanism. In some cases at lower laser powers, shock wave generation can also be produced by local absorption and fast thermal expansion, not requiring necessarily the occurrence of a plasma. Information on the kinetics of plasma has been usually achieved from time-resolved spectroscopy [15–17], luminescence [18] and interferometry [19], while photoacoustic and photomechanical phenomena have been investigated by means of piezoelectric transducers [20] and PVDF needle hydrophones [21, 22] that allow direct measurements of the peak pressure, and with diagnostics techniques, as pump–probe [23] and imaging arrangements [24–26]. In particular, time-resolved imaging of the different phases of laser–target interaction can provide useful information on the geometry and the evolution of pressure waves and cavitation bubbles, as required for the application of a suitable theoretical analysis. The interpretation of such laser-induced processes has been limited in the past by the relatively poor temporal resolution of the imaging set ups (usually employing flashlamps with duration of tens of microseconds), by the difficulty to extract quantitative information on the local behavior of physical parameters such as pressure, density and temperature with sufficient spatial resolution, and by the low reproducibility of measurements, especially when the investigations concerned biological tissues. For example, in the biomedical application of laser-induced fragmentation some remarkable issues are still debated, as the exact distribution of laser energy into the different process channels involved or the principal cause that leads to photodisruption [27, 21, 22].

In this work, we present a diagnostic technique that furnished time-resolved imaging of laser–target interaction with high temporal and spatial resolutions (10 ns and 20 μm, respectively). As an exemplary application, we studied photoablation and photofragmentation in artificial samples of kidney stones, with standardized physical

and chemical characteristics that ensured high reproducibility of measurements. The experimental results were analyzed by using the theoretical model of "point explosion" in liquid environment, originally developed by Sedov [28], that in our opinion can provide useful information also on the modelling of laser–target interactions. This theoretical approach has been recently proposed also by another group [29] to provide a qualitative interpretation of laser-induced photofragmentation, not directly supported by experimental validation. In the present research, we applied the "point explosion" model to analyze the observed kinetics of both shock wave and cavitation bubble, obtaining quantitative evaluations of the physical parameters associated with photoacoustic interaction, that cannot usually be measured directly.

1 Theoretical premises

The main hypothesis and results of the theoretical model of "point explosion" that have been applied to our experimental observation are briefly summarized here.

This model assumes the instantaneous release of a certain energy E_0 (explosion energy) in a point of a homogeneous ideal fluid. In the case of an incompressible liquid and for a sufficiently high value of E_0, the effects of this explosion are the expansion of a supersonic spherical pressure wave and the development of a cavitation bubble from the center of explosion. Considering an empty bubble and neglecting the counterpressure of the external liquid in respect to the peak pressure produced by the explosion (self-similar case), the cavitation radius obeys the following law of motion:

$$R = \left(\frac{E_0}{2\pi\rho_l}\right)^{1/5} t^{2/5}, \tag{1}$$

where ρ_l is the density of the liquid. The explosion energy E_0 can be regarded as the sum of two contributions: the cavitation energy $E_C = (4\pi/3)(p_l - p_V) R_{max}^3$, i.e. the energy required to move the liquid volume against the external pressure (where p_l is the static pressure of the unpertubed liquid, p_V is the equilibrium water vapor pressure inside the cavitation bubble and R_{max} the maximum bubble radius) and the energy associated to the pressure wave, regarded as the sum of kinetic and thermal contributions. This model does not account for chemical and radiative processes.

The pressure maximum is localized independently of the time at:

$$r_{max} = \sqrt[3]{4}\, R \tag{2}$$

and its dependence upon r is given by

$$p_{max} = \frac{3}{25\pi \sqrt[3]{4}} \frac{E_0}{r^3}. \tag{3}$$

After a certain time, when the external counterpressure of the liquid cannot be neglected in comparison with p_{max} (non-self-similar case), the kinetics of cavitation is described by the Rayleigh–Sedov equation:

$$\left(\frac{dR}{dt}\right)^2 = -\frac{2}{3}\frac{(p_l - p_V)}{\rho_l} + \frac{4}{25R^3}\left(\frac{E_0}{2\pi\rho_l}\right). \tag{4}$$

The steady-state solution of (4) gives the maximum cavitation radius:

$$R_{max} = \sqrt[3]{\frac{3}{25\pi}\frac{E_0}{(p_l - p_V)}}. \tag{5}$$

Incidentally, by comparing the expression of the cavitation energy E_C with (5), one can observe that according to Sedov's theory the energy associated to the cavitation bubble E_C results in $\frac{4}{25}$ of the whole explosion energy E_0 released into the fluid.

The general solution of (4) expressed through t is

$$t = \frac{3^{5/6}\sqrt{\rho_l}\, E_0^{1/3}}{(25\pi)^{1/3}\sqrt{2}(p_l - p_V)^{5/6}} \int_0^{\xi} \frac{d\xi}{\sqrt{1/\xi^3 - 1}}, \tag{6}$$

where $\xi = R/R_{max}$. This equation describes both the expansion and the collapse of the first cavitation cycle. Setting $\xi = 1$, it provides the expansion time, which is equal to the collapse time in the hypothesis that the spherical symmetry of the bubble is maintained over the whole cavitation cycle:

$$t_c = 0.915\, R_{max}\sqrt{\frac{\rho_l}{(p_l - p_V)}}. \tag{7}$$

For the application of the results of this theory to the real case of high-power laser–target interaction, one has to consider some suitable modifications. The first issue to be considered is that the target surface limits the motion of the liquid in a semi-space. Assuming point and instantaneous explosion on the surface of an ideal solid target (with infinite acoustic impedance), the expanding cavitation bubble can be reasonably expected to be of hemispherical shape. With this hypothesis, the above equations that are strictly valid in an infinite fluid can be simply applied to the present case dividing E_0 by a factor of 2 to account for the fraction of photomechanical energy released in the liquid semi-space. Moreover, in the last phase of the collapse a real cavitation originates a microjet which can play an important role for the final fragmentation effect. The impact pressure (the so-called "water hammer" pressure) of this jet is given by [30]

$$p_{wh} = \rho_l c_l v_j \frac{\rho_s c_s}{\rho_l c_l + \rho_s c_s} \approx \rho_l c_l v_j, \tag{8}$$

where c_l and c_s are the sound speed in the liquid and in the solid target, respectively, ρ_s is target density and v_j is the speed of the jet. The approximation on the right is valid whenever the acoustic impedance of the target is much greater than that of the liquid.

2 Materials and methods

2.1 Flash photo setup

Laser-induced photoablation and photofragmentation experiments to test our diagnostic and imaging technique have been performed with a long pulse XeCl excimer laser (308 nm, 150 ns FWHM, 150 mJ/pulse) suitably designed and constructed for high-energy transmission through

optical fibers and employed in urologic surgery and angioplasty [31]. It is clear that the utilization of such surgical excimer laser represents just an exemplary application of the diagnostic technique, that can be advantageously applied also to other pulsed-laser sources [32]. The experimental arrangement is shown in Fig. 1. The probe system is composed of another XeCl excimer laser of short pulse duration (10 ns, 30 mJ/pulse) pumping a dye laser (Rhodamine B, 600 nm, 10 ns). The collimated and expanded probe beam is sent parallel to the target surface to illuminate the liquid volume where photoacoustic phenomena take place. The two excimer lasers are synchronized by means of a two-stage trigger that allows continuous variation of the delay between the probe pulse and the excitation one, with a time jitter of about 10 ns. The image of the interaction volume is collected by a CCD camera connected to a computerized system for laser beam diagnostics.

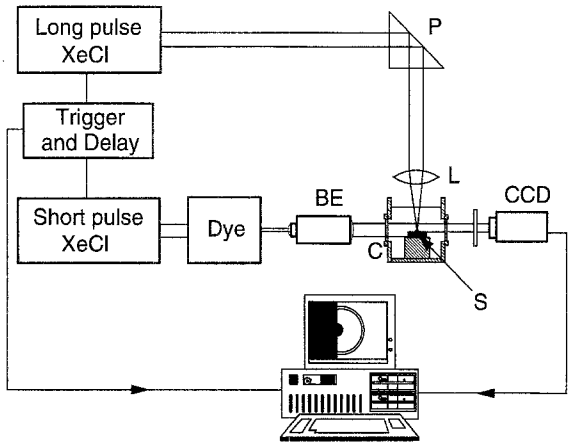

Fig. 1. Experimental set up. Legends: *BE*, beam expander: *C*, water cell; *S*, artificial sample; *P*, prism; *L*, focusing lens; *CCD*, video camera

2.2 Ablation targets

As targets we employed artificial samples of hard organic tissues. After some preliminary trials on real human kidney stones, we realized that the standardization of these models was mandatory to obtain a sufficient degree of reproducibility in our measurements. The importance of this requirement can be simply understood by considering that each frame recorded at a certain time delay is produced by a different laser pulse. Samples shaped like cylindrical tablets of 13 mm in diameter were prepared by compression from pure chemicals, as calcium phosphate and xanthine, typically present in human kidney stones, atherosclerotic plaques and bones. During laser irradiation, the targets were located in a water chamber with quartz windows on each side and submersed under 4 cm of distilled water. The beam of the long pulse XeCl laser was focused onto the target by a 10 cm focal length lens. The pulse energy was in the range 50–100 mJ, corresponding to energy fluences of 12–24 J/cm^2 at the focal spot (0.75×0.55 mm^2, as measured directly with a laser beam diagnostic system employing a CCD camera with pixel resolution of 11 μm and scaled up by considering beam refraction into water).

3 Results

The diagnostic system we arranged allowed direct visualization of the various phases of the photomechanical interaction. The evolution of an hemispherical pressure wave can be observed in the sequence of images reported in Fig. 2, obtained from a target of calcium phosphate

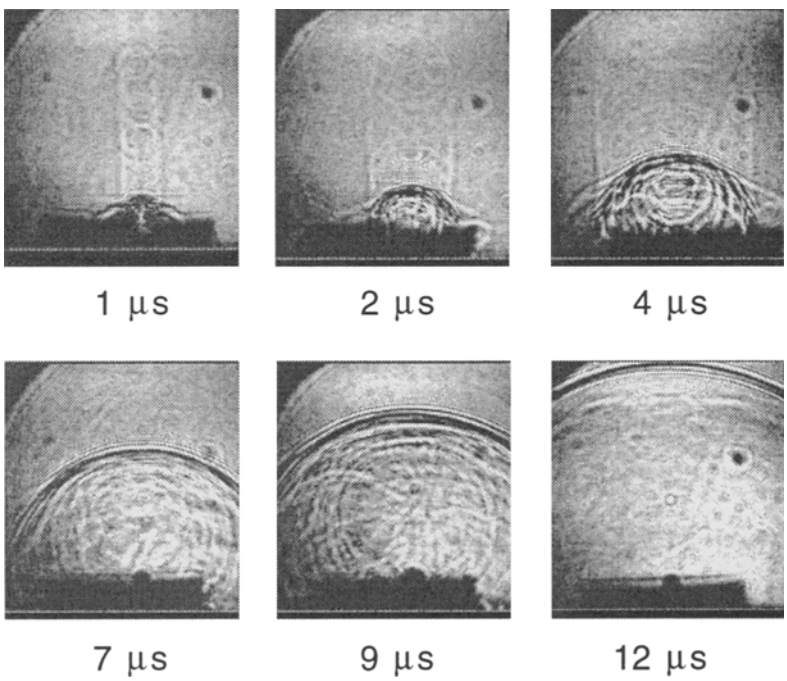

Fig. 2. Imaging of the pressure wave expansion and cavitation formation after XeCl laser irradiation on a target of calcium phosphate. Real image field is 18×20 mm

during the first 12 μs after laser irradiation. The observation field of each image is of about 18 × 20 mm. On this magnification scale, the formation of the cavitation bubble becomes visible in the center of explosion after about 4 μs. During this early phase, some secondary microshocks can casually occur near the sample surface (as better evidenced in the first two frames of Fig. 4), originated by water impurities and absorbing nuclei, that can cause some shielding effect, depending on their size and number.

The velocity of the shock front was evaluated by measuring the shock radius at different times. Figure 3 shows this plot for xanthine, evidencing the expansion of the pressure wave at supersonic speed for a few microseconds (about 2 μs, with reference to Fig. 3), then the speed decreases down to the sonic regime, corresponding in our case to a measured value of 1460 m/s.

The kinetics of cavitation was recorded and analyzed over a relatively long time range (about 1 ms) that included 2 or 3 cycles of bubble expansion and collapse. In all our observations we measured cavitation expansion and collapse velocities always lower than 300 m/s. This behavior indicates that the theoretical hypothesis of incompressible fluid is correct in our experimental conditions. In facts, as reported by Young [33], this assumption is strictly valid only up to $M \approx 0.2$ (where M is the Mach number defined as $\dot{R}/c_1$, being $\dot{R}$ and c_1 the cavitation expansion velocity and the sound velocity, respectively) that corresponds in water to $\dot{R} \approx 300$ m/s.

In calcium phosphate (Fig. 4, observation field of 4.5 × 5.0 mm) at a laser energy of 103 mJ/pulse, the bubble reaches a maximum radius of 3.5 mm in about 350 μs and then collapses, with the duration of the whole cycle of about 600 μs. A similar behavior was observed also in xanthine, but at a lower energy of 58 mJ/pulse, as shown in Fig. 5. Here the last 6 frames show also some images of the second cavitation cycle. In these sequences it can be noted that the hemispherical geometry of the cavitation bubble is kept along the whole cycle, except during the final phase of the collapse, when the bubble appears asymmetrical and presents significant squashing toward the target surface. In both the target types we succeeded in recording snapshots of the very instant of bubble collapse (see the 14th frame of both Figs 4 and 5), evidencing the formation of a rebound wave, that is usually strong enough to drive another subsequent cavitation cycle. The complex structure of this rebound wave, indicating a multiple origin of the second expansion, and the lack of spherical symmetry of the bubble observed in the final phase of the first cavitation cycle, provide qualitative arguments supporting the formation of a microjet at the end of bubble collapse. Sufficiently high reproducibility of cavitation radius measurements from time-resolved images resulted especially during the expansion phase (uncertainty on the cavitation radius ≈ 0.1 mm), confirming a good standardization in the physical and chemical properties of the artificial samples. On the other hand, significant time fluctuations of the second collapse event (that probably occurs around 850 μs) did not allow image recording of the second rebound wave.

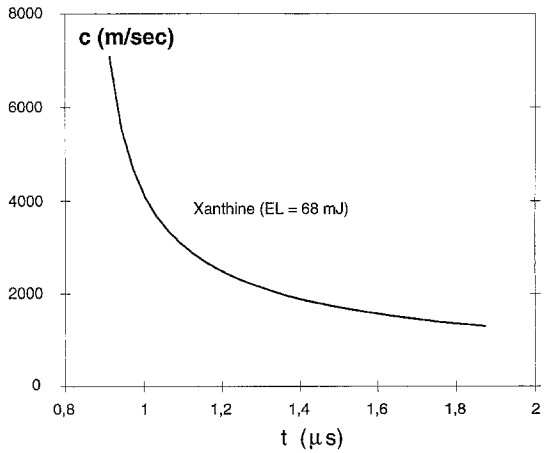

Fig. 3. Speed of the pressure wave produced by a XeCl pulse of 68 mJ on a target of xanthine

4 Analysis and comparison with theory

The physical parameter that characterizes the transfer of laser energy into photomechanical energy associated with both shock wave and cavitation formations is the explosion energy E_0. The value of this parameter can be calculated from our experimental measurements in two independent ways by using the (1) or (5), respectively. Table 1 reports the values of $E_0/2$ obtained with these two methods.

The first one requires to fit the observed cavitation kinetics with the self-similar law of motion (1), as shown in Fig. 6. The agreement is very good for the first 150 μs of bubble expansion, as long as the effects of the external counterpressure can be neglected.

The second method for to determining E_0 from (5) was based on the direct measurement of R_{max} from time-resolved imaging. The evaluation of this value was obtained with a higher precision in comparison with diagnostic techniques employing only hydrophones or other acoustic sensors. In fact, in those cases R_{max} is usually derived from (7) by measuring the time interval between the two pressure peaks corresponding to the beginning and the collapse of the bubble, with the implicit assumption that the spherical geometry is kept constant during the whole cavitation cycle, and expansion and collapse times are equal, while typically spatial and temporal instabilities at the end of the cycle break this symmetry.

With the different values of $E_0/2$ we plotted the evolution of the cavitation radius by using the general solution (6) of the Rayleigh-Sedov equation. The results are shown in Figs 7 and 8 for xanthine and calcium phosphate, respectively. The overall agreement with experimental data appears sufficiently good, especially in the expansion phase, where the spherical symmetry is well maintained. In particular, the calculated curve with $E_0/2$ derived from R_{max} seems slightly closer to the observed cavitation kinetics in comparison with the one obtained from the self-similar theory. Indeed, the relative uncertainty on the determination of $E_0/2$ is lower in the first case in respect to the second, depending on the powers of E_0 that appear in (1) and (5), respectively.

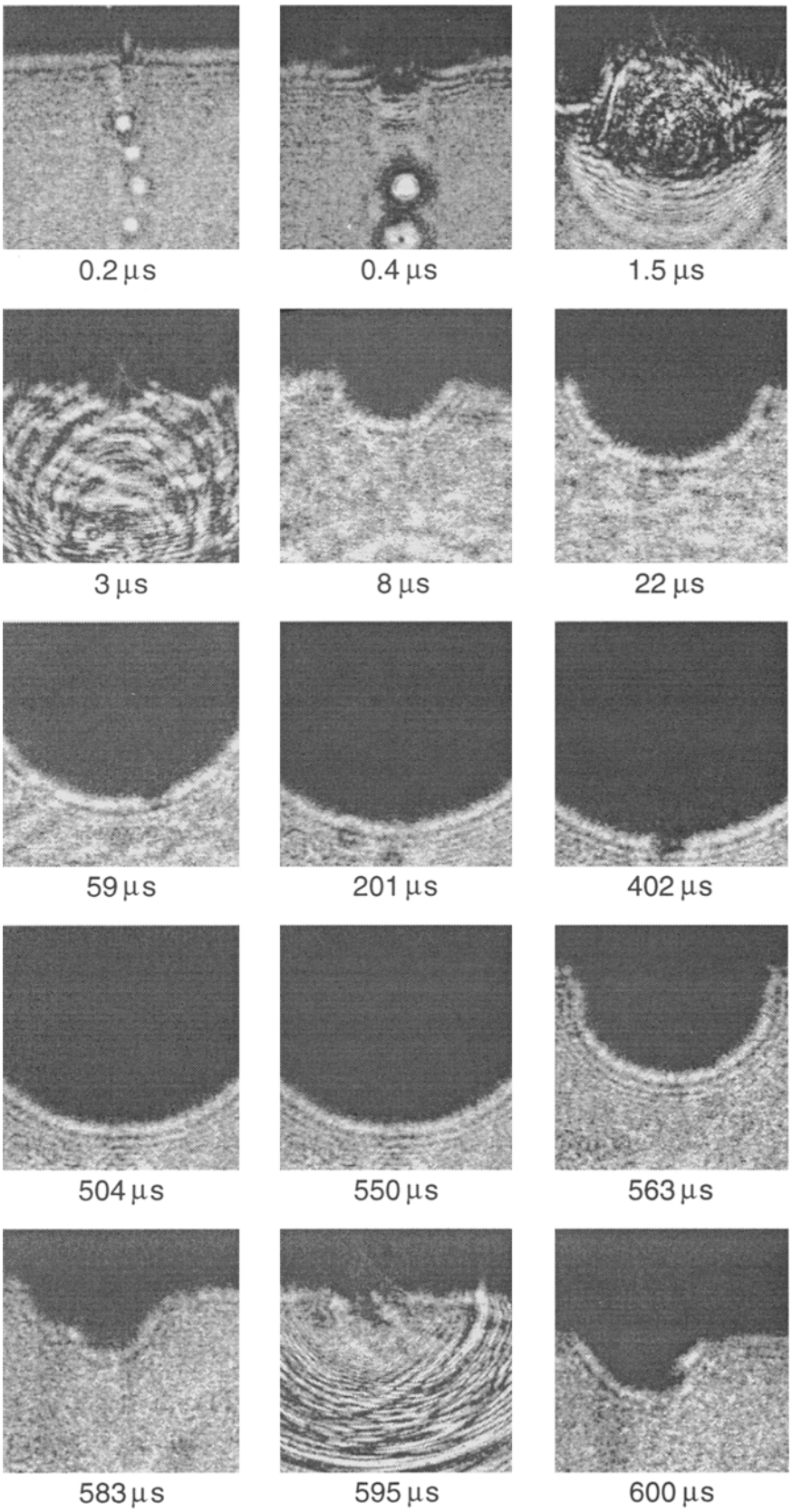

Fig. 4. Imaging of the cavitation kinetics induced by irradiation of calcium phosphate (XeCl laser energy of 103 mJ, image field of 4.5 × 5.0 mm)

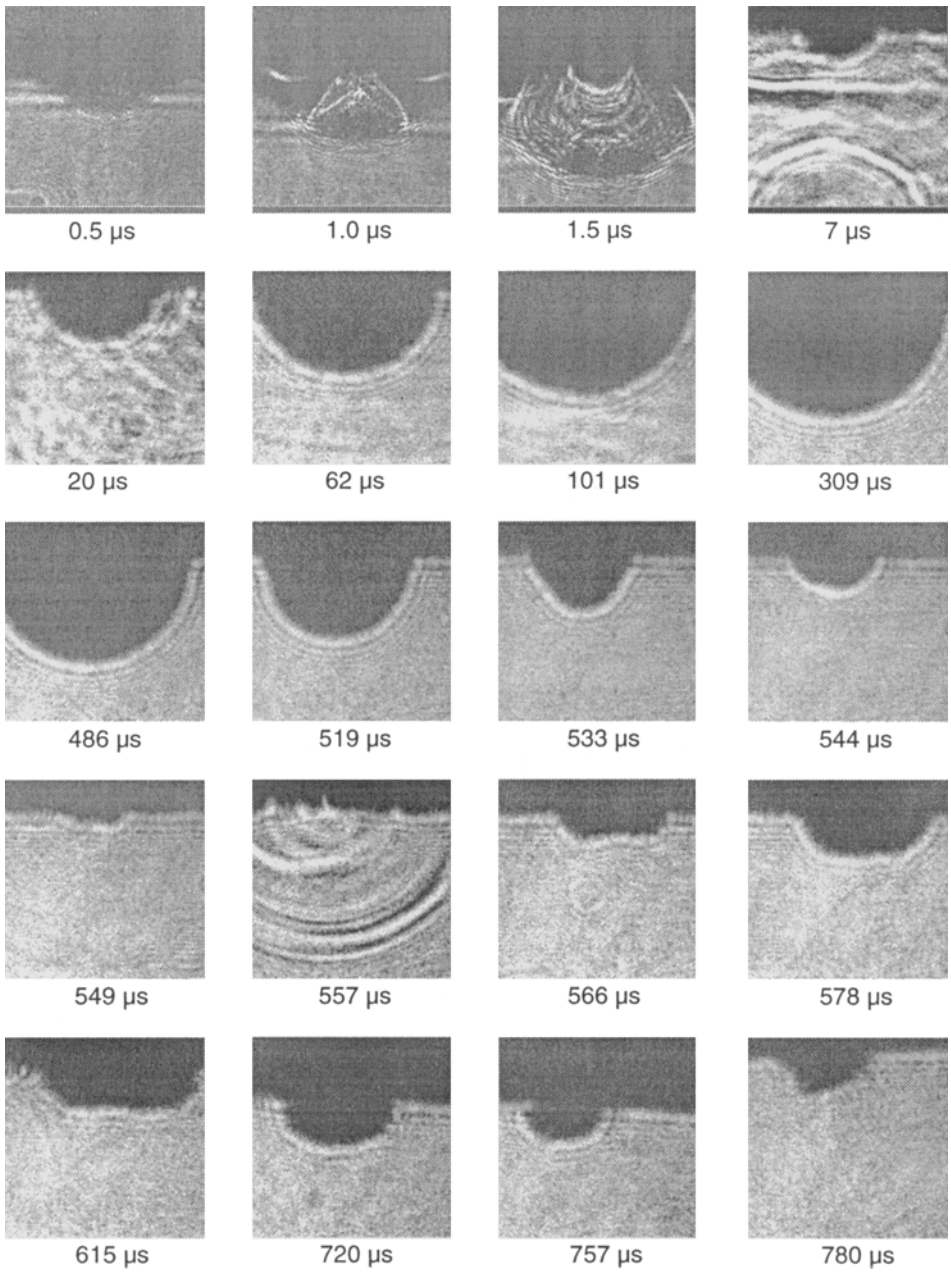

Fig. 5. Same as Fig. 4 but on a sample of xanthine irradiated with a laser energy of 58 mJ

Table 1. Calculated values of the explosion energy $E_0/2$ in the two sample types under test; E_L is the laser pulse energy and R_{max} the maximum caviation radius

Target type	E_L [mJ]	R_{max} [mm]	$E_0/2$ [a] [mJ]	$E_0/2$ [b] [mJ]
Calcium phosphate	103 (100%)	3.45	57.3 (56%)	53.6 (52%)
Xanthine	58 (100%)	3.10	30.2 (52%)	38.9 (67%)

[a] Self-similar case (evaluated from (1))
[b] Evaluated from R_{max} (5)

The results of this analysis point out that in our experimental condition the photomechanical energy coupling into the liquid, i.e. the energy transfer from the laser pulse to photoacoustic phenomena generated into water, is considerably high (50–70%, see Table 1). In our interpretation, the explosion energy can be practically represented by the whole thermomechanical energy, that includes the contributions due to pressure wave and cavitation formations, together with the fraction of energy that is lost in heat dissipative phenomena. Radiative energy losses are not included because the theory does not account for them, while the energy associated with the cloud of photoablated material can be considered in E_0, whenever this ejection plays some role to move the liquid and accelerate the cavitation kinetics. In this respect, the cavitation energy alone appears (that can be simply calculated as 0.16 $E_0/2$, resulting of 8.6 and 6.2 mJ for calcium phosphate and xanthine, respectively) as a small fraction of the explosion energy, even if it represents the potential energy of all the important phenomena occurring in the liquid at longer times, as rebound wave

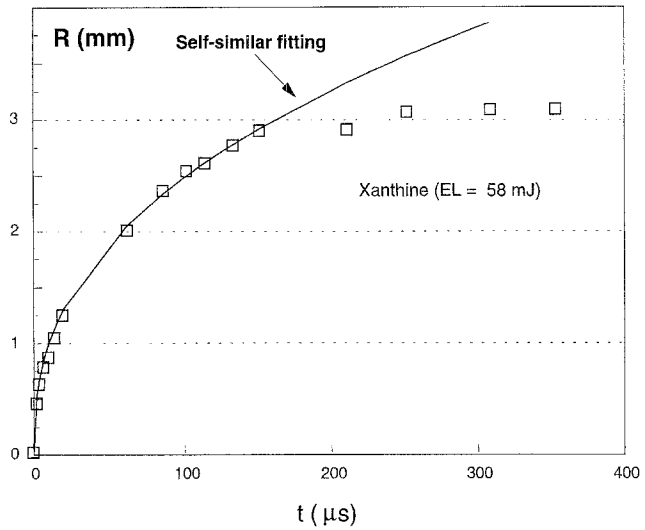

Fig. 6. Self-similar fitting of the evolution of the cavitation radius

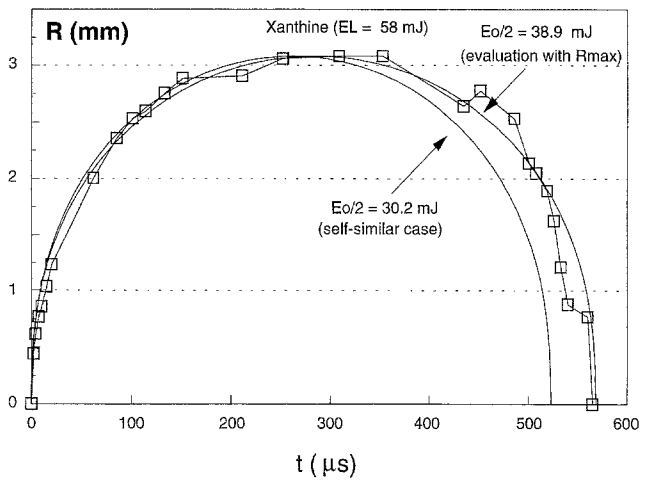

Fig. 7. Comparison of the cavitation kinetics observed after irradiation of Xanthine with two plots calculated according to (6), where the explosion energy E_0 was evaluated from R_{max} and from the self-similar fitting, respectively

formation and successive cavitation cycles. On the other hand, reports of direct measurements of the energy associated with the pressure wave, in various experimental conditions and with different lasers, indicate values smaller than 30% of the laser energy [34–36]. Considering these issues, it would be very interesting to identify the loss channels that dissipate the significantly high remaining fraction of E_0. The experimental study of these processes appears rather complex and will be the object of further investigations. What we can reasonably expect is that most of these energy losses take place in the very early phase of the process, when the pressure wave is expanding at supersonic speed and produces some compression of the liquid volume.

Regarding the prediction of the self-similar expression of the pressure maximum given by (3), we could not perform direct measurements of the pressure to verify its

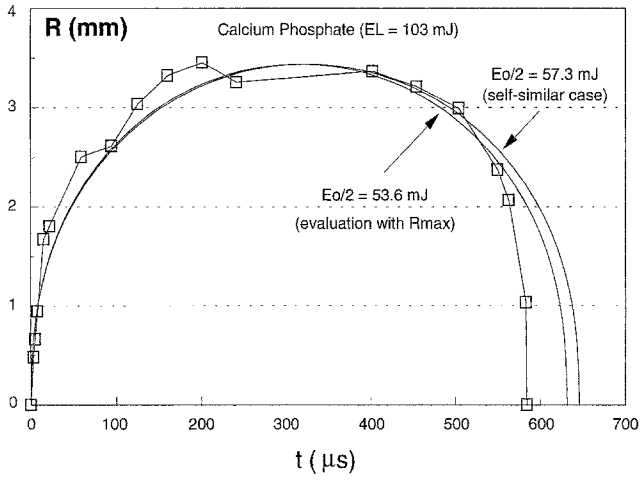

Fig. 8. Same as in Fig. 7, but in calcium phosphate

Table 2. Evaluation of the "water hammer pressure" onto the target surface produced by the microjet at the end of the cavitation bubble collapse; v_j is the estimated speed of the microjet

Target type	E_L [mJ]	v_j [m/s]	p_{WH} [bar]
Calcium phosphate	103	117	1730
Xanthine	58	74	1094

dependence upon r. Nevertheless, measurements of the ratio $r_{max}/R = \sqrt[3]{4}$ [see (2)] obtained from time-resolved pictures collected during the early microseconds indicated that this condition is generally no more valid after 2 μs, which leads one to also argue that (3) loses its validity after this time. This aspect is worth further researches concerning direct measurements of pressure transients.

In our analysis we considered an internal pressure p_V inside the bubble given by the static water vapor pressure at 15°C. This assumption of gas equilibrium is not strictly true, even if we expect that it does not alter substantially the kinetics in our experimental conditions.

The formation of a microjet in the last phase of the collapse was not directly observed with our probe configuration employing a collimated beam, but its occurrence is reasonably expected, according to previous works describing cavitation bubble generation near solid boundaries [37, 38]. In effect, the images of collapsing bubbles (13th frames of both Figs 4 and 5) seem to show that they are losing their hemispherical symmetry to acquire a bilobed shape with a pit in the middle. The pressure due to the jet impact onto the target surface was evaluated from (8), where as v_j we introduced the maximum speed value of the cavitation wall during bubble collapse (calculated by fitting experimental points), that can be assumed as the inferior limit of the jet speed. The results of this analysis are reported in Table 2.

5 Conclusions

The diagnostic setup we arranged for time-resolved imaging permitted a direct study of some laser-induced

acoustic phenomena involved in underwater photofragmentation of solid targets. In particular, the relatively high temporal resolution allowed the observation of the shock waves generated in water by the laser pulse and by the rebound occurring at the end of the cavitation collapse.

Measurements on shock wave and cavitation bubble evolution have been obtained with high experimental reproducibility. Detailed observations of the kinetics of these photoacoustic phenomena permitted their analysis by means of the Sedov's theory, where the classical Rayleigh's theory of cavitation is extended according to the theoretical model of point explosion in liquids. In this concern, we verified the self-similar kinetics of laser-induced cavitation bubbles up to 150 μs. The determination of the energy associated to the whole photoacoustic process (namely, the explosion energy E_0), here obtained and verified in two independent ways, can help to clarify the picture of the energy transfer from the laser pulse to the final fragmentation effect, furnishing new insights into the photoacoustic process channel in underwater laser-target interactions.

References

1. S.P. Dretler: Lasers Surg. Med. **8**, 341 (1988)
2. S. Mattioli, M. Cremona, G. Benaim, R. Salimbeni, R. Pini: In *Laser Deposition of Advanced Materials*, ed. by M. Allegrini, A. Giardini Guidoni, A. Modrone (Edizioni ETS, Pisa 1992) pp. 226–228
3. W. Shi, T. Papaioannou, L. Daykhovsky, S.G. Vari, W.S. Grundfest: Lasers Surg. Med. **10**, 284 (1990)
4. A. Vogel, W. Hentshel, J. Holzfuss, W. Lauterborn: Ophthalmology **93**, 1259 (1986)
5. F. Docchio, P. Regondi, M.R.C. Capon, J. Mellerio: Appl. Opt. **27**, 3661 (1988)
6. B. Zysset, J.G. Fujimoto, T.F. Deutsch: Appl. Phys. B **48**, 139 (1989)
7. A.D. Zweig, T.F. Deutsch: Appl. Phys. B **54**, 76 (1992)
8. T.F. Deutsch: In *Laser Deposition of Advanced Materials*, ed. by M. Allegrini, A. Giardini Guidoni, A. Modrone (Edizioni ETS, Pisa 1992) pp. 201–203
9. K. Dörschel, G. Müller: SPIE Proc. **1525**, 253 (1991)
10. P. Teng, N.S. Nishioka, R.R. Anderson, T.F. Deutsch: IEEE J. QE-**23**, 1845 (1987)
11. O. Yavas, P. Leiderer, H.K. Park, C.P. Grigoropoulos, C.C. Poon, W.P. Leung, N. Do, A.C. Tam: Appl. Phys. A **58**, 407 (1994)
12. S. Siano, F. Margheri, P. Mazzinghi, R. Pini, R. Salimbeni, M. Vannini: Tech. Dig. Int.'l Conf. Lasers 95, Charleston, USA (1995) paper THA.1
13. C.E. Bell, J.A. Landt: Appl. Phys. Lett. **10**, 46 (1967)
14. P.A. Barnes, K.E. Rieckhoff: Appl. Phys. Lett. **13**, 282 (1968)
15. I.S. Fishman, G.G. Il'in, M.Kh. Salakhov: J. Phys. D **20**, 728 (1987)
16. N.S. Nishioka, P. Teng, T.F. Deutsch, R.R. Anderson: Lasers Life Sci. **1**, 231 (1987)
17. J. Helfmann: Untersuchung der physikalischen Phänomene bei der Zertrümmerung von Körperkonkrementen durch laserinduzierte Plasmen. Dissertation, Freie Universität Berlin (1991)
18. F. Docchio: Europhys. Lett. **6**, 407 (1988)
19. M. Vest: In *Optical Metrology*, ed. by O.D.D. Soares, NATO ASI Ser. (Nijhoff, Dordrecht 1987) pp. 343–364
20. R.O. Esenaliev, A.A. Oraevsky, V.S. Letokhov, A.A. Karabutov, T.V. Malinsky: Lasers Surg. Med. **13**, 470 (1993)
21. K. Rink, G. Delacrétaz, R.P. Salathé: Appl. Phys. Lett. **61**, 258 (1992)
22. K. Rink, G. Delacrétaz, R.P. Salathé: Appl. Phys. Lett. **61**, 2644 (1992)
23. A.G. Doukas, A.D. Zweig, J.K. Frisoli, R. Birngruber, T.F. Deutsch: Appl. Phys. B **53**, 237 (1991)
24. M.B. Preisack, W. Neu, R. Nyga, M. Wehrmann, K.K. Haase, K.R. Karsch: Lasers Surg. Med. **12**, 520 (1992)
25. P.E. Dyer, M.E. Khosroshahi, S.J. Tuft: Appl. Phys. B **56**, 84 (1993)
26. T. van Leeuwen: In *Bubble Formation During Pulsed Mid-Infrared and Excimer Laser Ablation: Origin and Implications for Laser Angioplasty* (CIP-gegevens Koninklijke Bibliotheek, den Haag 1993)
27. G. Müller, J. Helfmann, V.P. Pashinin, P.P. Pashinin, V.I. Konov, V.V. Tumorin, E.J. Shklosvsky: SPIE Proc. **2086**, 103 (1993)
28. L.I. Sedov: In *Similarity and Dimensional Methods in Mechanics* (CRC, Boca Raton 1993) Chap. 4
29. J. Helfmann, V.A. Mihailov, V.I. Konov, G. Müller, D.A. Nikolaev, S.K. Pak, I.A. Shcherbakov, A.S. Silenok: SPIE Proc. **1643**, 80 (1992)
30. G. Hammitt: In *Cavitation and Multiphase Flow Phenomena* (McGraw-Hill, New York 1980) p. 221
31. R. Salimbeni, R. Pini, M. Vannini, G. Benaim, S. Mattioli: SPIE Proc. **2084**, 280 (1993)
32. R. Pini, R. Salimbeni, S. Siano, G. Toci, M. Vannini: Tech. Dig. Int.'l Conf. Lasers 94, Quebec City, Quebec, Canada (1994) paper THD. 5
33. F.R. Young: In *Cavitation* (McGraw-Hill, London 1989) Chap. 2, p. 26
34. M.K. Sigrist: J. Appl. Phys. **60**, R83 (1986)
35. K.L. Vodop'yanov, L.A. Kulevskii, V.G. Mikhalevich, M.A. Rodin: Sov. Phys.-JETP **64**, **67** (1986)
36. H. Shoeffmann, H. Schmidt-Kloiber, E. Reichel: J. Appl. Phys. **63**, 46 (1988)
37. F.G. Hammit: In *Cavitation and Multiphase Flow Phenomena* (McGraw-Hill, New York 1980) Chap. 5
38. A. Vogel, W. Lauterborn: J. Acoust. Soc. Am. **84**, 719 (1988)